NMR Solution Structure of Plastocyanin from the Photosynthetic Prokaryote, *Prochlorothrix hollandica*[†,‡]

Charles R. Babu,[§] Brian F. Volkman,[∥] and George S. Bullerjahn*[,§]

Center for Photochemical Sciences, Department of Biological Sciences, Bowling Green State University, Bowling Green OH, 43403, and Nuclear Magnetic Resonance Facility at Madison, Department of Biochemistry, University of Wisconsin, Madison WI 53706

Received December 23, 1998; Revised Manuscript Received March 1, 1999

ABSTRACT: The solution structure of a divergent plastocyanin (PC) from the photosynthetic prokaryote *Prochlorothrix hollandica* was determined by homonuclear ^{1}H NMR spectroscopy. Nineteen structures were calculated from 1222 distance restraints, yielding a family of structures having an average rmsd of 0.42 ± 0.08 Å for backbone atoms and 0.71 ± 0.07 Å for heavy atoms to the mean structure. No distance constraint was violated by more than 0.26 Å in the structure family. Despite the low number of conserved residues shared with other PC homologues, the overall folding pattern of *P. hollandica* PC is similar to other PCs, in that the protein forms a two-sheet β-barrel tertiary structure. The greatest variability among the backbone structures is seen in the loop region from residues 47−60. The differences seen in the *P. hollandica* PC homologue likely arise due to a small deletion of 2−4 residues compared to the PC consensus; this yields a less extended loop containing a short α-helix from residues Ala52−Leu55. Additionally, the protein has an altered hydrophobic patch thought to be important in binding reaction partners. Whereas the backbone structure is very similar within the loops of the hydrophobic region, the presence of two unique residues (Tyr12 and Pro14) yields a structurally different hydrophobic surface likely important in binding *P. hollandica* Photosystem I.

Plastocyanin (PC)[1] is a small (∼10 kDa), Type 1 copper protein that functions as an electron donor to Photosystem I (PSI) from cytochrome (cyt) *f* in both chloroplast systems and in some strains of cyanobacteria (*1*−*3*). In some lower eukaryotes and most cyanobacteria, a small *c*-type cytochrome serves this function (*4*, *5*), and many of these organisms can synthesize both components, replacing PC with cyt c_6 under conditions of copper limitation (*6*−*8*). PCs from cyanobacterial and chloroplast sources can be classified into several classes, depending on their origin and primary structure (*2*). Whereas the chloroplast PC homologues exhibit a great deal of similarity at the level of primary structure, the cyanobacterial PCs are highly variable with respect to sequence and isoelectric point. Due to such variability, only 18 amino acids are universally conserved across this family of proteins (*2*), yet all retain a common tertiary structure and coordinate a single Cu ion near a hydrophobic region at the "top" of the molecule. The binding site is defined by a cysteine, a methionine, and two histidine residues that form a distorted tetrahedral cage. His87 of poplar PC is a surface-exposed residue surrounded by the hydrophobic patch; it is likely that this residue yields the electron transport pathway into the PSI acceptor. In sum, PCs are β-sheet polypeptides that act as electron carriers having a midpoint redox potential of approximately +350 mV (*1*−*3*).

A wealth of structural information is available on the chloroplast PC homologues; indeed, X-ray crystal structures are available for PC from poplar (*9*, *10*), spinach (*11*), *Enteromorpha* (*12*), and *Chlamydomonas* (*13*) and NMR solution structures have been determined for French bean (*14*), parsley (*15*), and *Scenedesmus* (*16*) PCs. By comparison, there are comparatively little data on the PCs from the cyanobacteria; at this writing, the solution structure of *Anabaena* (*17*) and a crystal structure of a triple mutant of *Synechocystis* (*18*) PC are the only structures available. Given the differences in primary structure between the chloroplast and cyanobacterial PCs, as well as the high degree of variability among the cyanobacterial PC homologues, we have sought to determine the structure of PC from the photosynthetic prokaryote, *Prochlorothrix hollandica*. This PC is the most divergent member of the protein family known; it has only 31% identity and 44% similarity to poplar and 35% identity and 56% similarity to *Synechocystis* PC

[†] Work at Bowling Green was supported by NSF Grant MCB-9634049 awarded to G.S.B. NMR studies were carried out at the National Magnetic Resonance Facility at Madison with support from NIH Biomedical Technology Program (RR02301) and additional equipment funding from the University of Wisconsin, NSF Academic Infrastructure Program (BIR-9214394), NIH Shared Instrumentation Program (RR02781, RR08438), NSF Biological Instrumentation Program (DMB-8415048), and USDA.

[‡] Coordinates for the refined average structure and the family of 19 structures have been deposited in the Protein Data Bank under the codes 1B3I and 2B3I, respectively.

* To whom correspondence should be addressed. Tel: +1 (419) 372-2333. E-mail: bullerjahn@opie.bgsu.edu.

[§] Bowling Green State University.

[∥] University of Wisconsin−Madison.

[1] Abbreviations: PC, plastocyanin; PSI, Photosystem I; cyt, cytochrome; NOE, nuclear Overhauser effect; NOESY, NOE spectroscopy; TOCSY, total correlation spectroscopy; DQF−COSY, double-quantum filtered correlation spectroscopy; FID, free induction decay; τ_m, mixing time; TAD, torsion angle dynamics.

10.1021/bi983024f CCC: $18.00
Published on Web 04/01/1999

(*19*). This likely reflects the positioning of *P. hollandica* as a deeply branched member of the cyanobacteria (*20*).

Two major structural features of PCs are the presence of two regions thought to be involved in binding the reaction partners: the aforementioned hydrophobic patch on the top of the molecule in the vicinity of the His87 (in poplar PC) Cu ligand, and a negative patch composed of acidic amino acids common to chloroplast PCs, but absent in the cyanobacterial PC homologues. Whereas PCs in general all have a hydrophobic region, *P. hollandica* PC has a hydrophobic patch that is uniquely and substantially different at the level of amino acid sequence (*19*). For example, the conserved amino acid residues in poplar involved in forming the hydrophobic patch are Gly10, Leu12, Pro36, His87, and Ala90; indeed, Gly10 and Leu12 have been targets for site-directed mutagenesis in examining the role of this region in interactions with cyt *f* and PSI (*21*−*23*). Since these two residues were initially believed to be invariant in all PCs, we were quite surprised to find that the *P. hollandica* PC has a tyrosine (Tyr12) and a proline (Pro14) residue at these respective positions (*19*). Determination of the solution structure of *P. hollandica* PC and comparison to other known structures may help reveal the minimum structural features required for reaction partner binding and productive electron transfer.

EXPERIMENTAL PROCEDURES

Sample Preparation. Prochlorothrix hollandica apoPC was synthesized in *Escherichia coli*, purified, and reconstituted with Cu *in vitro* as described previously (*24*). The reduced form of PC was produced from pure PC by reduction with an excess of sodium dithionite. All experiments were performed on samples in 20 mM potassium phosphate buffer at pH 7.0 in 90% H_2O/10% D_2O or 99.9% D_2O. The sample for D_2O experiments was prepared by lyophilizing and redissolving the protein in D_2O. Final protein concentrations were 2−4 mM. Throughout this paper, amino acid positions are numbered according to the *P. hollandica* PC, unless otherwise stated.

NMR Spectroscopy. All NMR spectra were recorded at 25 °C on a Bruker DMX750 spectrometer equipped with three-axis pulsed field gradient capabilities. Quadrature detection in the indirectly detected dimensions was obtained with the States-TPPI method (*25*). Two-dimensional NOESY, TOCSY, and DQF−COSY experiments were acquired in both H_2O and D_2O with the spectral width of 11363.64 Hz for both dimensions. The NOESY and TOCSY experimental data consisted of 1024 t_2 and 512 t_1 complex points. DQF−COSY data consisted of 2048 t_2 and 512 t_1 complex points. NOESY spectra were acquired with mixing times of 75 and 150 ms in H_2O and 100 ms in D_2O (*26*). TOCSY spectra were acquired with spinlock periods of 83.2 ms (*27*). Solvent suppression for 2D NOESY and TOCSY experiments in 90% H_2O was achieved with a 3-9-19 watergate sequence (*28*, *29*). Presaturation was used for suppression of the residual solvent signal in NOESY and TOCSY experiments collected in D_2O. Gradient pulses as a combination of X- and Z-gradients at the "magic angle" (*30*, *31*) were used for coherence selection and water suppression in the 2D DQF−COSY experiment. The TOCSY spectrum (256 t_1 experiments) acquired immediately after dissolving the protein in D_2O was used to identify the slowly exchanging amide protons. The recording time was 2 h.

NMR data processing and analysis were performed in Felix 95 or 97 (Molecular Simulations, San Diego, CA). Typically, a deconvolution function was used to remove the residual water signal and 75°-shifted skewed sinebell window function was applied to each FID prior to zero filling and Fourier transformation. The final matrix size was 2048 × 2048 except for DQF−COSY which was 4096 × 4096. The spectra were referenced assuming 4.80 ppm for the water signal.

Distance Constraints. Peak picking was done using the Stella peak picking routine in Felix. Peaks in overlapping regions were manually edited. Peak volumes were calculated using Felix in the NOESY spectrum acquired in H_2O (τ_m = 75 ms) and in the D_2O (τ_m = 100 ms). The DYANA (*32*) readable peak volume list was obtained by using a Perl script. In DYANA, volumes were calibrated by using CALIBA (*33*) to get upper distance bounds. NOESY peak volumes from water and D_2O experiments were calibrated independently. Standard calibration was performed using backbone, side-chain, and methyl classes. Only the scalar for the backbone calibration class was adjusted interactively.

Copper Restraints. The copper atom was included in the structure calculations as a residue linked to the C-terminus of the protein using several linker residues as explained in the DYANA manual (*34*). A van der Waals radius of 0.5 Å was used to avoid the van der Waals violation between the copper atom and the ligands. The copper coordination geometry was found to be similar to that found in other plastocyanins from resonance Raman spectroscopy (Dr. Joann Sanders-Loehr and Dr. Linda Cameron, personal communication). Thus, it was assumed that the copper is coordinated by the same ligands as in other plastocyanins, namely, His39Nδ, Cys82Sγ, His85Nδ, and Met90Sδ. The coordination of copper by Nδ of histidines and not by Nϵ is confirmed by the observation of His39-N$^{\epsilon}$H and His85-N$^{\epsilon}$H at 11.49 and 11.24 ppm, respectively. Taking this into account, we used previously established bond distance and angle restraints in the form of lower and upper bound restraints in the structure calculations (*14*). The restraints of 2.05 ± 0.05, 2.05 ± 0.05, 2.30 ± 0.05, and 2.90 ± 0.05 Å with the relative weight of 10 were used for Cu−His39Nδ, Cu−His85Nδ, Cu−Cys82Sγ, and Cu−Met90Sδ bond distances. Similarly, the angles Cu−N−C (127°) and Cu−S−C (120°) with the relative weight of 10 and X−Cu−X (110°) where X = N or S with the relative weight of 5 were restrained.

Structure Calculations. Structures were calculated by simulated annealing using torsion angle dynamics (TAD) in the program DYANA starting from random conformers (*32*). Typically, 20 structures with the lowest target function values were analyzed out of 40 structures calculated. For each structure 4000 TAD steps were performed at high temperature T_{high} = 8.0 (target function units), followed by slow cooling to the final temperature T_{end} = 0.0, during 16 000 TAD steps. This cooling stage was followed by 1000 steps of conjugate gradient minimization. In the final refinement, the conjugate gradient minimization was followed by a multilevel variable target function minimization (*33*). Structure calculations and peak assignments were done iteratively. Stereospecific assignments for beta protons of prolines and

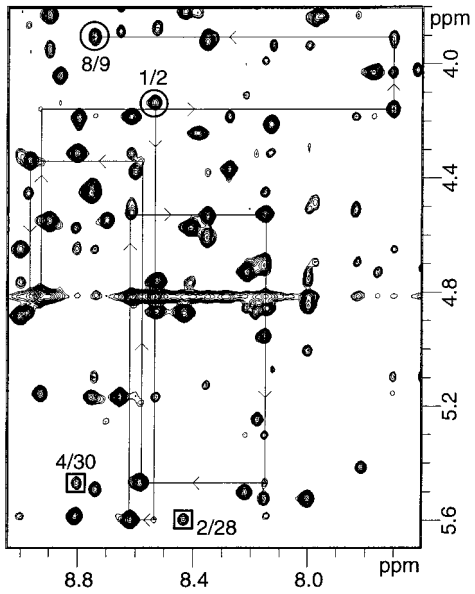

FIGURE 1: Sequence-specific resonance assignment for amino acids 1−9. The NOESY spectrum (τ_m = 75 ms) acquired in H_2O at pH 7.0 and 25 °C is shown. The series of alternating inter- and intraresidue connectivities are shown by arrows. The first and the last $d_{\alpha N}(i,i+1)$ cross-peaks in the series are marked by circles. Interstrand $d_{\alpha N}(i,j)$ cross-peaks are indicated by squares.

side-chain amide protons of Asn and Gln were obtained manually on the basis of NOEs (*35*). After several iterations of structure calculations, GLOMSA was used to obtain more stereospecific assignments (*33*). The average structure was calculated in MOLMOL after superimposing the final 19 structures on backbone atoms of residues 3−97 (*36*). This average structure was regularized by using a multilevel variable target function minimization in DYANA (*33*). The criteria for hydrogen bond analysis were the following: ∠NHO = ±35° from linearity and the distance H···O ≤ 2.6 Å. The same criteria are used when the donor and/or acceptor are different from N or O. Programs Insight II (Molecular Simulations, San Diego, CA) and MOLMOL (*36*) were used in structure visualization and analysis.

RESULTS

Sequence-Specific Resonance Assignments. A wealth of assignment information is available for plastocyanins from variant species. Resonance assignments were obtained by following the standard procedures (*37*). The TOCSY spectrum in combination with DQF−COSY was used to identify the spin systems. All valines, 8 of 9 threonines, 9 alanines, and most of the glycines were identified from the unique spin systems. The remaining glycines and Ala1 at the N-terminus were identified at the sequence-specific resonance assignment stage. Aromatic amino acids, 2 of 3 asparagines, and one glutamine were identified using NOESY data. After categorizing the remaining spin systems into several groups, we made sequence-specific assignments for the regions with the series of strong $d_{\alpha N}$ connectivities in NOESY. Ambiguities due to chemical shift degeneracy were resolved by the $d_{\beta N}$ connectivities. Then, the sequence-specific assignments were obtained for the connecting regions and prolines. The region of the NOESY spectrum showing the $d_{\alpha N}$ connectivities for amino acids 1−9 is shown in Figure 1. The spin systems for Ser66 and His85 (one of the Cu ligands) were assigned on the basis of the NOE peaks to their sequential neighbors, since the backbone amide resonances for these amino acids were not observed. This was confirmed by TOCSY and by the observation of NOEs between ring and aliphatic protons for His85. Last, the stretch of amino acids from Asn57 to Ala63 was assigned. This was left unassigned until the end because of the discrepancies in the amino acid sequence deduced from the DNA sequence and the NMR data. From the NMR data, it was found that Arg61 should be Ala61. Therefore, the plasmid DNA used for protein expression was resequenced independently by automated sequencing. This sequence data showed that the original codon sequence was GCT, instead of the previously reported CGT (*19*). This codon change confirms the expected protein sequence error.

cis-Prolines. In all plastocyanins, Pro18 and Pro38 have *cis* conformations (*9*−*18*). The presence of a *cis* X-Pro peptide bond is easily detected in a 2D NOESY spectrum with the observation of a strong cross-peak between the alpha protons of the proline and the preceding residue. Only a weak αH−αH sequential NOE is observed for the *cis* peptide bond of Pro18, since the αH chemical shifts of both Glu17 and Pro18 are near the solvent signal which is suppressed by presaturation in the D_2O NOESY. However, a sequential NOE between Glu17 NH and Pro18 αH confirms that the Pro18 is in the *cis* conformation. For the Pro38, NOEs between alpha protons of Gly37 and Pro38, and Gly37 NH and Pro38 αH are observed, confirming that Pro38 is also in the *cis* conformation.

Secondary Structure. Secondary structure elements can be identified on the basis of the short- and medium-range connectivities shown in Figure 2. The series of strong $d_{\alpha N}$ connectivities together with the presence of slowly exchanging amide protons indicate *β*-strands as a prevalent secondary structure. The observation $d_{\alpha N}(i,i+3)$ and $d_{\alpha\beta}(i,i+3)$ connectivities in the regions 51−56 and 86−90 suggest the presence of short α-helices.

Structure Calculations. After calibrating the integrated NOESY peaks by using CALIBA, we obtained a total of 1622 unique upper distance limits (*33*). After removing trivial distance restraints and correcting others by adding pseudo-atom corrections in DYANA, we obtained a total of 1222 (220 intraresidual, 332 sequential, 125 medium-range, and 545 long-range) upper distance restraints. This corresponds to an average of 12.6 restraints per residue. The distribution of the NOE distance restraints per residue along the sequence is shown in Figure 3. As mentioned in the experimental procedures, in addition to the NOE-derived upper distance restraints, 14 upper and 14 lower distance restraints were used to define the copper geometry. No hydrogen bond or dihedral angle restraints were used in the calculation. Apart from the 9 stereospecific assignments obtained manually for prolines, asparagines, and glutamine, the preliminary structures from DYANA were used to obtain 12 more stereospecific assignments using GLOMSA (*33*). These assignments along with chemical shifts and restraints were also submitted to the Brookhaven Protein Data Bank.

The stereoview of the final family of 19 out of 40 structures calculated in DYANA is shown in Figure 4. The final family of 19 structures has an average rmsd of 0.42 ± 0.08 Å for backbone atoms and 0.71 ± 0.07 Å for heavy atoms (except the first two residues) to the mean structure.

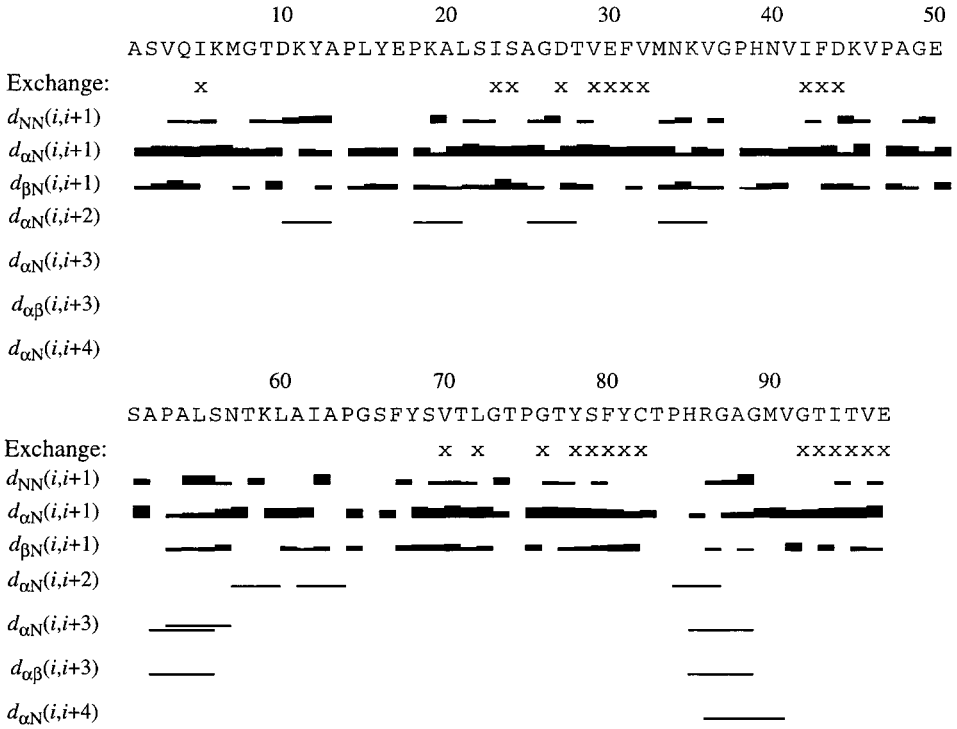

FIGURE 2: Summary of the sequential and medium-range NOE connectivities involving HN, Hα, and Hβ protons. The thickness of the bar represents NOESY cross-peak intensity. Slowly exchanging amide protons are shown by X.

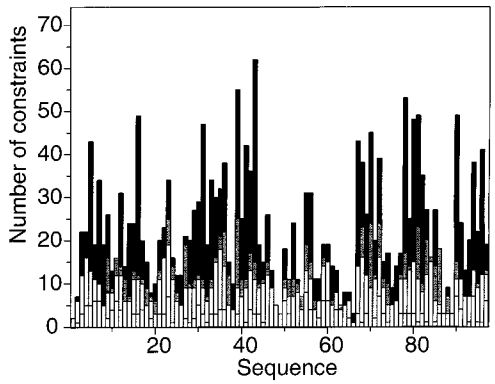

FIGURE 3: Number of meaningful intraresidue (white), sequential (light gray), medium-range (dark gray), and long-range (black) NOE-derived distance restraints per residue versus the amino acid sequence.

No distance constraint was violated by more than 0.26 Å in the structure family. The target function values ranged from 0.38 to 0.76 Å^2 with an average of 0.59 ± 0.12 Å^2. These indicate that the family of structures agrees well with the NOE data and the structures have been well-defined. In addition to the backbone conformation, the side chains of amino acids forming the hydrophobic core inside are very well-defined. The average structure calculated from the family has a target function value of 0.36 Å^2 after refinement by variable target function minimization in DYANA. This minimized structure has an average pairwise rmsd of 0.52 ± 0.12 Å for backbone atoms and 0.95 ± 0.14 Å for heavy atoms (except the first two residues) to the family. Structural statistics of the family of structures and the refined average structure are summarized in Table 1. A Ramachandran plot analysis in DYANA for the final family of structures shows that only His85 and Arg86 fall in the disallowed region in one of the 19 structures. It is important to point out that the backbone amide resonance for His85 was not observed. Table 2 summarizes the Ramachandran statistics for the family of conformers and for the refined average structure.

Hydrogen Bonds. Twenty five slowly exchanging amides were identified in the TOCSY spectrum (Figure 2). Among these, 22 residues (5, 23, 29−32, 42, 44, 70, 72, 76, 78−82, and 92−97) are in the β-strand regions involved in forming parallel or antiparallel β-sheets. The amide protons of these residues except for 31, 42, 76, 79, and 93 form hydrogen bonds with the carbonyl oxygens of the counter strand in 8 or more structures. Among the remaining three slowly exchanging amides, the amide proton of Ser24 is involved in a hydrogen bond with a side-chain carboxylate oxygen of Asp27 in all 19 conformers. The hydrogen bond Asp27 HN···OC Ser24 was also observed in all 19 structures. For the Phe43 HN, the hydrogen bond acceptor was identified as Ser56 γO in only one structure. Several backbone amide protons forming consistent hydrogen bonds in the calculated structures are not significantly protected from deuterium exchange.

The resonances of seven OH protons and two histidine side-chain NH protons are observed in the NMR spectra, indicating a decreased exchange rate. Among these, hydrogen bonds between Tyr16 ηH···OC Tyr81 and His39 ϵNH··· OC Lys35 are observed in 6 and 18 structures, respectively. The Ser56γOH, as in other PCs, is even observed in DQF−COSY and TOCSY experiments. However, a consensus hydrogen bond acceptor is not identified for the Ser56γOH in the family of conformers. Similarly, for the remaining slowly exchanging protons, potential hydrogen bond acceptors are identified only in few structures.

DISCUSSION

Overview of the Structure. In this paper, we report the three-dimensional structure of a divergent prokaryotic plastocyanin. Due to sequence variability among all PCs analyzed

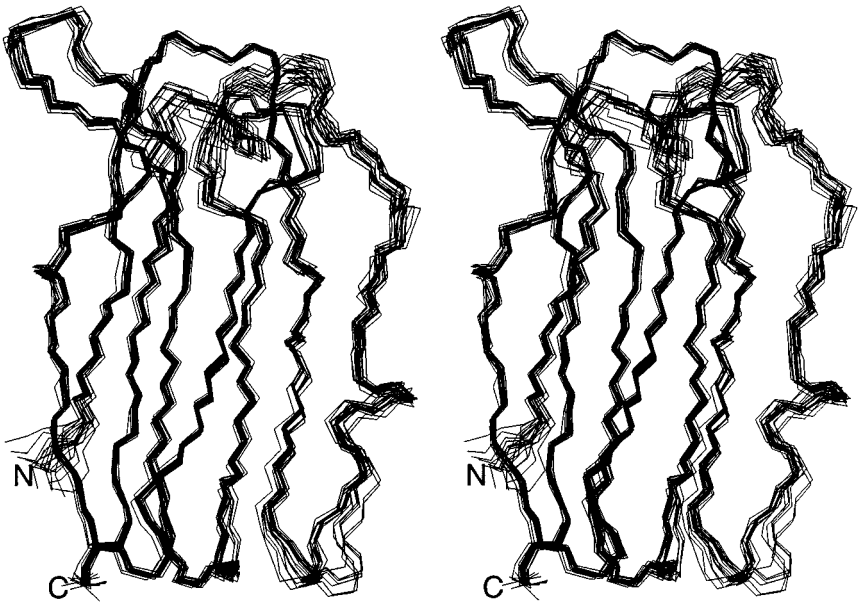

FIGURE 4: Stereoview of the 19 selected structures of *P. hollandica* plastocyanin superimposed on the backbone (N, C^{α}, and C′) atoms of residues 3−97. The copper atom is not shown.

Table 1: Structural Statistics for the Family of 19 Structures and the Refined Average Structure

parameter	family	average
average target function (Å^2)	0.59 ± 0.12	0.36
backbone rmsd[a] (Å)	0.42 ± 0.08	n/a
all heavy atom rmsd (Å)	0.71 ± 0.07	n/a
largest upper restraint violation (Å)	0.26	0.14
largest van der Waals violation (Å)	0.22	0.16
average of the sum of upper restraint violations (Å)	3.3 ± 0.6	2.3
average of the sum of van der Waals violations (Å)	2.5 ± 0.4	1.6

[a] rmsds were calculated for residues 3−97.

Table 2: The Ramachandran[a] Plot Statistics for the Family of 19 Structures and the Refined Average Structure

	family	average
percentage of residues in		
most favored regions (%)	63.0	62.3
additionally allowed regions (%)	33.4	35.1
generously allowed regions (%)	3.5	2.6
disallowed regions (%)	0.1	0.0

[a] Glycines, prolines, and the end residues were not included in the statistics.

to date, only a minority of residues are conserved across the protein family. Nonetheless, the *P. hollandica* PC structure exhibits a global folding pattern very similar to both chloroplast and cyanobacterial PCs. As seen in the schematic representation of the refined average structure (Figure 5; the strands are numbered as in ref *15*), the protein is composed of eight β-strands organized in two sheets. Sheet 1 is composed of strands from residues 3−9, 15−17, 28−34, and 68−72; the β-strands of sheet 2 include the residues from 20 to 23, 42 to 45, 76 to 81, and 91 to 97. Apart from the β-sheets, a short helix from Ala52 to Leu55 is present. Helical hydrogen bonds Leu55 NH···OC Ser51 and Ser56 NH···OC Ala52 are observed in 18 and 15, respectively, out of 19 calculated structures. In addition to these hydrogen bonds, Ala54 NH···OC Ala52 is also observed in 14 structures, probably due to the presence of proline at location 53.

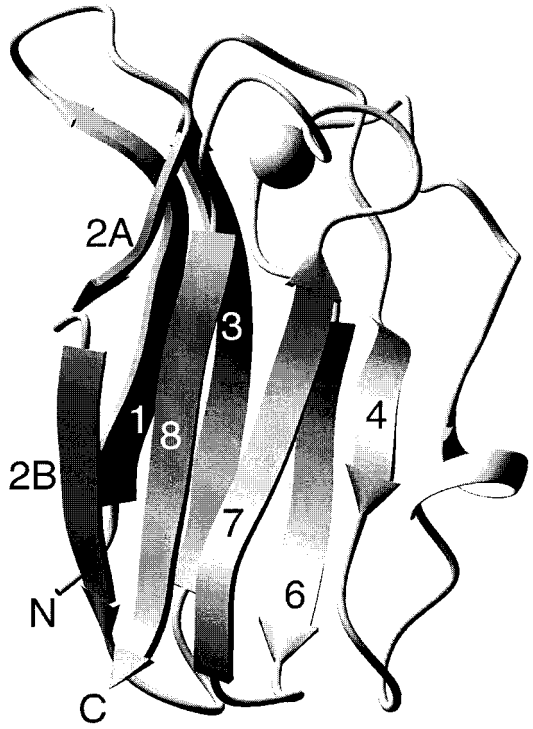

FIGURE 5: Schematic representation of the *P. hollandica* plastocyanin structure. Labels indicate the β-strand numbers as in ref *15*. The copper atom is indicated by the sphere. The structure figures were created in MOLMOL (*36*).

Comparison to Other PC Homologues. The sequence alignment aided by the poplar, *Synechocystis*, and *P. hollandica* PC structural comparisons is shown in Figure 6. For direct comparison, the superposition of *P. hollandica*, *Synechocystis* sp. (PDB no. 1PCS) and poplar (PDB no. 5PCY) PC structures is also shown (Figure 7). Even though the global fold of the three proteins is very similar, a few structural differences can be pointed out. First, the β-strand from *P. hollandica* residues 42−45 (strand 4 in Figure 5) is shorter by comparison. As a result, although strong $d_{\alpha N}$ NOE connectivities are observed, a short strand comprising

```
Poplar     --IDVLLGADDG SLAFVPSEFS[20] ISPGEKIVFK NNAGF[35]
Synech.    ANATVKMGSDSG ALVFEPSTVT[22] IKAGEEVKWV NNKLS[37]
P. holl.   ATVQIKMGTDKY APLYEPKALS[22] ISAGDTVEFV MNKVG[37]
                       *   *
Poplar       PHNIVFDEDS IPSGVDASKI[55] SMSEEDLLNA KGETF[70]
Synech.      PHNIVFAADG VDA-DTAAKL[56] SHK--GLAFA AGESF[69]
P. holl.     PHNVIFDK-- VPAGESAPAL[55] SNT--KLAIA PGSFY[68]

Poplar       EVALSNKGEY SFYCSPHQGA[90] GMVGKVTVN[99]
Synech.      TSTFTEPGTY TYYCEPHRGA[89] GMVGKVVVE[98]
P. holl.     SVTLGTPGTY SFYCTPHRGA[88] GMVGTITVE[97]
```

FIGURE 6: Amino acid sequence alignment of plastocyanins from poplar, *Synechocystis*, and *P. hollandica*, aided by structural comparisons. The residues forming the hydrophobic patch in the three-dimensional structure are indicated in bold. The starred (*) residues denote unique changes in the *P. hollandica* sequence.

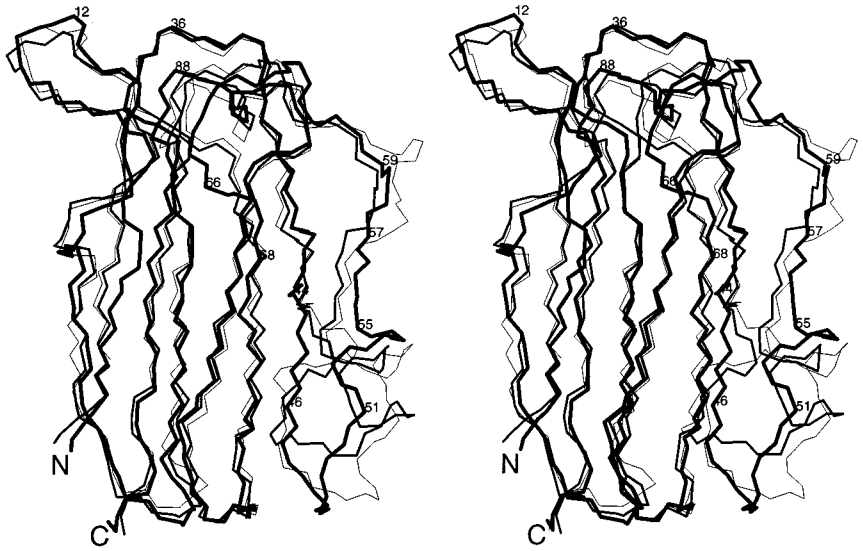

FIGURE 7: Stereoview of the superposition of *P. hollandica* (bold line), *Synechocystis* (thick line), and poplar (thin line) PCs. The backbone (N, C^{α}, and C′) atoms corresponding to residues 3−44 and 61−97 of *P. hollandica* were superimposed. The *P. hollandica* PC residue numbers are indicated.

residues 60−62 reported in other PC structures (*15*) is missing standard interstrand connectivities with strand 4, and these residues do not adopt a β-strand conformation. Second, the β-strand from residues 68−72 is also shorter, yielding a displacement of the backbone centered at Ser66 (Figure 7). Third, the extended loop region containing the chloroplast PC negative patch (residues 47−60) exhibits the greatest variability among the PC homologues. Compared to other PCs, *P. hollandica* PC has a small deletion of 2−4 residues (centered on position 45) immediately prior to the loop (Figure 6). The effect of this deletion is a less extended loop region containing a four residue helix; the *Synechocystis* homologue has a longer helix within the loop (Figure 7). Since the small (92 residue) PC recently discovered from *Synechococcus* has a more extensive deletion in this region (*38*), we speculate that the *Synechococcus* homologue will lack the short helix altogether. Fourth, as in *Synechocystis* and green algae PCs, a two residue deletion present in the *P. hollandica* PC prevents the formation of the characteristic bulge normally observed in plant PCs at residues 58−60 (corresponding to poplar PC) (Figures 6, 7). Fifth, note that the position of the two short deletions in the *P. hollandica* PC variable loop region roughly correspond to the positioning of the negatively charged patch that is characteristic of higher plant PCs (Figure 6). Last, in the *P. hollandica* PC, regarding His39 (one of the copper ligands), the $C^{\epsilon}H$ (6.95 ppm) is found further downfield than $C^{\delta}H$ (6.75 ppm) as is typical for histidines. However, in the plastocyanin structures solved thus far, $C^{\delta}H$ (∼7.5 ppm) has been found further downfield than $C^{\epsilon}H$ (∼7.1 ppm) for the corresponding histidine. Additionally, for the first time, the $N^{\epsilon}H$ of His85, a second copper ligand, has been observed at 11.24 ppm. The carbonyl oxygen of Val36 is in close proximity to the $N^{\epsilon}H$ of His85, suggesting the possible hydrogen bond analogous to the other copper ligand (His39) as a reason for the unusual pK_a of this proton.

Characteristics of the Hydrophobic Patch. The major unique structural feature of *P. hollandica* PC is the presence of an altered hydrophobic patch yielded by the presence of Tyr12 and Pro14 corresponding to the highly conserved Gly10 and Leu12 (poplar numbering) that have been targets for site-directed mutagenesis (see alignment, Figure 6). Prior work on chloroplast PC has shown the importance of Gly10 and Leu12 on both binding and electron transport with PSI and cyt *f* reaction partners (*21*−*23*). Comparison of the backbone structures presented in Figure 7 reveals that Tyr12 and Pro14 of *P. hollandica* PC do not greatly alter the loop region contributing to the hydrophobic patch. However, a space-filling model of the hydrophobic patch yields a highly altered surface conformation (Figure 8). In all 19 structures,

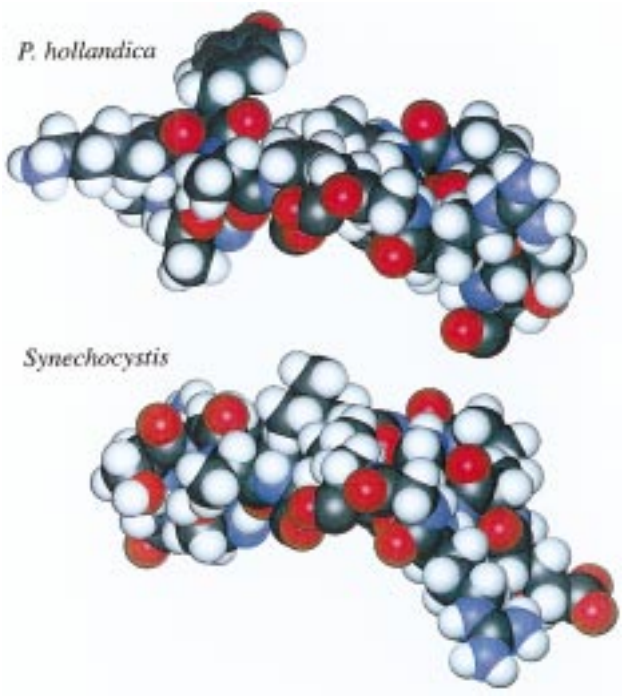

FIGURE 8: Space-filling model of the hydrophobic patches of *P. hollandica*, and *Synechocystis* PCs. The orientation and superposition is the same as in Figure 7. After superimposition, one of the molecules was moved along the *y*-axis for clarity. Only the residues 9−14, 35−40, and 83−88 of *P. hollandica* PC and the corresponding residues in the *Synechocystis* PC are shown.

Tyr12 is surface-exposed and extends outward from the hydrophobic patch.

Concluding Remarks. Kinetic analyses of electron transport from *P. hollandica* plastocyanin and *P. hollandica* PSI occur by a Type II mechanism, in which a stable complex is formed prior to electron transport (*39*). *P. hollandica* PC does not form a complex with chloroplast or *Anabaena* PSI. Further experiments suggest a strong dependence on hydrophobic interactions in complex formation with *P. hollandica* PSI, given the 80% decrease in the observed rate constant following the addition of glycerol to 10% (*39*). This is in contrast to PC/PSI reaction pairs in other cyanobacteria, in which glycerol addition has comparatively little effect. It is possible that the properties of the altered hydrophobic surface present in *P. hollandica* PC yield the observed dependence on hydrophobic interactions mediating the formation of a PC/PSI complex. Future mutagenesis studies will target Tyr12 and Pro14 of *P. hollandica* PC in experiments aimed at converting the hydrophobic patch to allow productive electron transfer to heterospecific PSI preparations as well as maximizing hydrophobic interactions to *P. hollandica* PSI. Last, comparison of *P. hollandica* PSI reaction center and cyt c_6 primary structures should also reveal the domains that have coevolved to yield the sites responsible for the protein−protein interactions necessary for productive electron transport.

ACKNOWLEDGMENT

The authors thank Prof. Miguel A. De la Rosa (University of Seville) and his colleagues for the laser flash kinetic studies and helpful discussions regarding PSI/PC interactions. Thanks also to Drs. Joann Sanders-Loehr and Linda Cameron (Oregon Health Sciences Center) for performing the resonance Raman spectroscopy. Automated sequencing of the cloned *petE* plasmid was performed by E. Sonay Kuloglu (University of Wisconsin−Madison).

REFERENCES

1. Sigfridsson, K. (1998) *Photosynth. Res. 57*, 1−28.
2. Gross, E. L. (1996) in *Oxygenic Photosynthesis: The Light Reactions* (Ort, D. R., and Yocum, C. F., Eds.) pp 413−429, Kluwer Academic Publishers, Dordrecht, The Netherlands.
3. Redinbo, M. R., Yeates, T. O., and Merchant, S. (1994) *J. Bioenerg. Biomembr. 26*, 49−66.
4. Wood, P. M. (1978) *Eur. J. Biochem. 87*, 9−19.
5. Ho, K. K., and Krogmann, D. W. (1984) *Biochim. Biophys. Acta 766*, 310−316.
6. Sandmann, G. (1986) *Arch. Microbiol. 145*, 76−79.
7. Merchant, S., and Bogorad, L. (1986) *Mol. Cell Biol. 6*, 462−469.
8. Arudchandran, A., and Bullerjahn, G. S. (1996) *Biochem. Biophys. Res. Commun. 226*, 626−630.
9. Guss, J. M., and Freeman, H. C. (1983) *J. Mol. Biol. 169*, 521−563.
10. Guss, J. M., Harrowell, P. R., Murata, M., Norris, V. A., and Freeman, H. C. (1986) *J. Mol. Biol. 192*, 361−387.
11. Xue, Y. F., Okvist, M., Hansson, O., and Young, S. (1998) *Protein Sci. 7*, 2099−2105.
12. Collyer, C. A., Guss, J. M., Sugimura, Y., Yoshizaki, F., and Freeman, H. C. (1990) *J. Mol. Biol. 211*, 617−632.
13. Redinbo, M. R., Cascio, D., Choukair, M. K., Rice, D., Merchant, S., and Yeates, T. O. (1993) *Biochemistry 32*, 10560−10567.
14. Moore, J. M., Lepre, C. A., Gippert, G. P., Chazin, W. J., Case, D. A., and Wright, P. E. (1991) *J. Mol. Biol. 221*, 533−555.
15. Bagby, S., Driscoll, P. C., Harvey, T. S., and Hill, H. A. (1994) *Biochemistry 33*, 6611−6622.
16. Moore, J. M., Case, D. A., Chazin, W. J., Gippert, G. P., Havel, T. F., Powls, R., and Wright, P. E. (1988) *Science 240*, 314−317.
17. Badsberg, U., Jorgensen, A. M. M., Gesmar, H., Led, J. J., Hammerstad, J. M., Jespersen, L. L., and Ulstrup, J. (1996) *Biochemistry 35*, 7021−7031.
18. Romero, A., De la Cerda, B., Varela, P. F., Navarro, J. A., Hervas, M., and De la Rosa, M. A. (1998) *J. Mol. Biol. 275*, 327−336.
19. Arudchandran, A., Seeburg, D., Burkhart, W., and Bullerjahn, G. S. (1994) *Biochim. Biophys. Acta 1188*, 447−449.
20. Bullerjahn, G. S., and Post, A. F. (1993) *CRC Crit. Rev. Microbiol. 19*, 43−59.
21. Modi, S., Nordling, M., Lundberg, L. G., Hansson, O., and Bendall, D. S. (1992) *Biochim. Biophys. Acta 1102*, 85−90.
22. Nordling, M., Sigfridsson, K., Young, S., Lundberg, L. G., and Hansson, O. (1991) *FEBS Lett. 291*, 327−330.
23. Haehnel, W., Jansen, T., Gause, K., Klosgen, R. B., Stahl, B., Michel, D., Huvermann, B., Karas, M., and Herrmann, R. G. (1994) *EMBO J. 13*, 1028−1038.
24. Babu, C. R., Arudchandran, A., Hille, R., Gross, E. L., and Bullerjahn, G. S. (1997) *Biochem. Biophys. Res. Commun. 235*, 631−635.
25. Marion, D., and Wüthrich, K. (1983) *Biochem. Biophys. Res. Commun. 113*, 967−974.
26. Macura, S., Huang, Y., Suter, D., and Ernst, R. R. (1981) *J. Magn. Reson. 43*, 259−281.
27. Bax, A., and Davis, D. G. (1985) *J. Magn. Reson. 65*, 355−360.
28. Piotto, M., Saudek, V., and Sklenar, V. (1992) *J. Biomol. NMR 2*, 661−665.
29. Sklenar, V., Piotto, M., Leppik, R., and Saudek, V. (1993) *J. Magn. Reson., Ser. A 102*, 241−245.
30. VanZijl, P. C. M., Johnson, M. O., Mori, S., and Hurd, R. E. (1995) *J. Magn. Reson., Ser. A 113*, 265−270.

31. Warren, W. S., Richter, W., Andreotti, A. H., and Farmer, B. T. (1993) *Science 262*, 2005−2009.
32. Güntert, P., Mumenthaler, C., and Wüthrich, K. (1997) *J. Mol. Biol. 273*, 283−298.
33. Güntert, P., Braun, W., and Wüthrich, K. (1991) *J. Mol. Biol. 217*, 517−530.
34. Güntert, P., Mumenthaler, C., and Herrmann, T. (1998) in *DYANA User's Manual, Version 1.5*, Instutut für Molekularbiologie und Biophysik, Eidgenössische Technische Hochschule, Zürich, Switzerland.
35. Kline, A. D., Braun, W., and Wüthrich, K. (1988) *J. Mol. Biol. 204*, 675−724.
36. Koradi, R., Billeter, M., and Wüthrich, K. (1996) *J. Mol. Graphics 14*, 51−55.
37. Wüthrich, K. (1986) in *NMR of Proteins and Nucleic Acids*, Wiley, New York.
38. Clarke, A. K., and Campbell, D. (1996) *Plant Physiol. 112*, 1551−1561.
39. Navarro, J. A., Hervas, M., Babu, C. R., Molina-Heredia, F. P., Bullerjahn, G. S., and De la Rosa, M. A. (1998) in *Advances in Photosynthesis Research* (Garab, G., Ed.) Kluwer Academic Publishers, Dordrecht, The Netherlands (in press).

BI983024F